# Shape-stable and Smart Polyrotaxane-based Phase Change Materials with Enhanced Flexibility and Fire-safety

Guang-Zhong Yin,[a, b] Alba Marta López, [a] Xiao-Mei Yang, [a] Wen Ye, [a, c, d] Baoyun Xu, [c] Jose Hobson,[a] De-Yi Wang [a, b*]

[a] *IMDEA Materials Institute, C/Eric Kandel, 2, 28906, Getafe, Madrid, Spain*

[b] *Universidad Francisco de Vitoria, Ctra. Pozuelo-Majadahonda Km 1.800, 28223, Pozuelo de Alarcón, Madrid, Spain*

[c] *State Key Laboratory of Polyolefins and Catalysis, Shanghai Engineering Research Center of Functional FR Materials, Shanghai Research Institute of Chemical Industry Co. LTD., Shanghai, 200062, China*

[d] *Universidad Politécnica de Madrid, 28040, Madrid, Spain*

**Corresponding Author**

*Tel: +34 91 549 34 22, fax: +34 91 550 30 47; Email: deyi.wang@imdea.org

**Abstract**

With the high performance of intelligent electronic machines and the popularity of flexible and foldable devices and high-speed/large capacity 5G communication, the market demand for flexible heat storage and smart temperature control materials are gradually rising. Therefore, phase change materials (PCMs) have received much attention in the related energy storage and temperature control field. As the amount of PCM increases, so do the fire safety concerns associated with their applications. Therefore, the development of improved the flexibility and fire safety for advanced PCMs is imperative. In this work, we reported a pentaerythritol phosphate modified sustainable polyrotaxane as PCMs for thermal energy storage and thermal management. The structure of pentaerythritol phosphate was adequately confirmed by $^{13}C$ NMR, $^{31}P$ NMR and ATR-FTIR. Subsequently, the tensile properties, fire safety, phase change performances and shape memory properties of the PCMs were fully analyzed. The results showed that all the flexibility, fire safety and thermal conductivity of modified polyrotaxanes were enhanced remarkably compared to those of pristine polyrotaxane. Further with the high form stability, and excellent cycle stability, the modified polyrotaxanes are therefore promising sustainable and fire safe shape-stable PCMs for thermal energy storage. Notably, its ultra-high flexibility (with elongation higher than 1000 %), processing ability, excellent form-stability, enhanced fire-safety (with UL94 V-0 rating

and LOI of 33.0%) and thermal conductivity (0.47 W $m^{-1}$ $K^{-1}$) provide a practical way for the safe and intelligent heat treatment for some electronic devices, such as solid-state disk.

**Keywords**: Thermal Energy Storage, Polyrotaxane, Sustainable Phase Change Materials, Shape Memory Materials

## Introduction

With the high performance of intelligent electronic machines and the popularity of high-speed/large capacity 5G communication, the market demand for heat storage and smart temperature control materials are gradually rising. Therefore, phase change materials (PCMs) have received much attention in the related energy storage and temperature control field. [1-3] PCMs with high latent heat have been extensively used for heat management aspect. [4] However, it is still a great challenge to apply heat management for wearable devices using PCMs due to their solid rigidity and liquid leakage. [5] Some promising efforts have been dedicated to fabricate flexible PCMs by blending PCMs with different flexible polymers. [6-8] The design and fabrication of intrinsically flexible PCMs is also explored. [9] Recently, a new kind of sustainable, flexible and shape-stable polyrotaxane (PLR) based PCM was reported in our group. [10] As the amount of PCMs increases, so do the safety concerns associated with their application. However, the PCMs (including the PLR based PCMs) are easily flammable due to the chemical constitutions of conventional PCMs and supporting materials, which is still the main restrain for the wide and practical applications. Thus, the development of improved the fire safety for advanced PCMs is also imperative.

Several methods have been attempted to reduce the PCM flammability. Anyway, introducing fire safe additives into PCMs is still the most widely used method to improve the fire safety of PCMs. [11-16] For example, Cai et al. [4] reported that Magnesium hydroxide, microencapsulated red phosphorus and organic montmorillonite contributed to form a compact and homogeneous char residue and thus improve the thermal property and flammability of PCMs. Intumescent flame retardants can be applied in PCMs because of their advantages of good safety and relatively high flame retarding efficiency. The method involves encapsulating it inside a composite building block and then placing the block inside a hollow container surrounded by non-combustible concrete. Some others have tried impregnating PCM into gypsum wallboard [5]. Generally, acid source, char-forming agent, and blowing agent are incorporated into formulations to obtain intumescent flame retardancy. [13] As it is reported, Cyclodextrin is a good carbon source in the combustion process. [17, 18] It can be expected the introduction of acid sources can be a great improvement in terms of fire safety, especially the char forming ability.

Melamine salts of pentaerythritol phosphate (MPP) were prepared from the reactions of pentaerythritol with phosphorus oxychloride/or phosphoric acid and melamine are highly efficient flame retardants by acting acid source and they were used to improve the flame retardancy of Polypropylene (PP), [19] thermoplastic polyurethane [20], cotton fabric, [21] and polyurethane foam. [22] In order to obtain good dispersion, a water soluble and halogen-free additive is suitable. Furthermore, the oil-like modifier may act as an inter-pore bridge to form a contact region, which ensures high mechanical properties even under a high filling content. It is difficult for rigid particles (with non-deformability) to implement many filler modifications with well dispersion. Moreover, it can increase the processing difficulty and decrease the flexibility of polymer matrix itself due to the poor compatibility between rigid particles and PCM matrix. [23] As we know, energy storage and electronic devices are developing towards flexible and intelligent, which requires a higher mechanical strength and flexibility of materials. [9, 24] It is further reported that the introduction of multiple hydrogen bonds into hydroxy-rich polymer may enable the corresponding polymer to possess promising mechanical properties. [25] Different hydrogen bonding reinforced factors have been employed for polymer preparation to fabricate of supramolecular hydrogels mediated by hydrogen bonds. [26-28] Therefore, to fulfill mechanical enhancement and good dispersion, we will directly use polyhydroxy oil flame

retardant modifier, Pentaerythritol phosphate (PPP) as acid source to modify PLR based PCMs. It is expected that good dispersion and mechanical strengthening can be promoted and the fire safety of the material can be improved on the premise of satisfying the excellent process ability and flexibility. The pathway here can effectively avoid high temperature processing or problems related to the dispersion of other particles. Moreover, the introduction of small molecule additives with good compatibility may increase the density of materials and improve the thermal conductivity, which will greatly contribute to the performance of materials in the heat treatment of electronic devices.

In this work, we will prepare the bio-based supramolecular phase change materials and use PPP as a modifier to improve the fire safety. The optical, mechanical, thermal properties, fire safety, shape memory properties, phase change behaviors and a typical application of the PCMs will be fully investigated.

## Results and discussion

### *1. Preparation and investigation of PPP modified PLR (PLR-P)*

PPP was synthesized by a solvent free method and the details for synthesis are provided in Experimental section (see the Supplementary Material). The chemical structure of PPP was fully confirmed by FTIR, $^{31}$P NMR and $^{13}$C NMR spectra (**Figure S1-S3**). The assignment of the spectra was all provided in **Table S1-S2**. The obtained PPP (**Figure 1a**) is water soluble mixture of cyclic and exocyclic structure and blended directly with the PLR by using water as a solvent, giving rise to the PPP modified PLR (PLR-P) (**Figure 1b**). UV-Vis spectra were firstly used to detect transmittance of the PLR and PLR-Ps (**Figure S4**). All the PCM films had a high transmittance of about 80 % at 400-800 nm, indicating the addition of PPP didn't make the PLR transparency change significantly. The FTIR spectra of all the PCMs are also recorded and provided in **Figure S5**. There is no significant difference among all the modified PLRs and pristine PLR.

Both PPP and PLR are water-soluble and belong to polyhydroxy compounds. The hydrogen bond interaction can make sure the good compatibility between PPP and PLR, so as to facilitate the dispersion of PPP in the PLR matrix. PLR-P50 was chosen as a typical example for the PPP dispersion analysis (**Figure 1c**). There are two kinds of morphologies in Figure 1c. The red region is the part without significant aggregation of PPP, as further illustrated in **Figure 1d**; while the purple region is with significant aggregation of PPP, as illustrated in **Figure 1e**. Due to the oil-like characteristics and water solubility, the PPP has good compatibility and is easy to be dispersed in PLR. Therefore, even if aggregation existed (Sample PLR-P50, Figure 1c), only micro-nano scale aggregations were formed in partial region. As shown in **Figure 1f**, the average particle size is only about 220 nm (The detail of the corresponding data treatment was described in supplementary materials, see **Figure S6**). Moreover, the Energy Dispersive Spectrometer (EDS) results (**Figure 1g**) directly proved the dispersion state of PPP in PLR matrix.

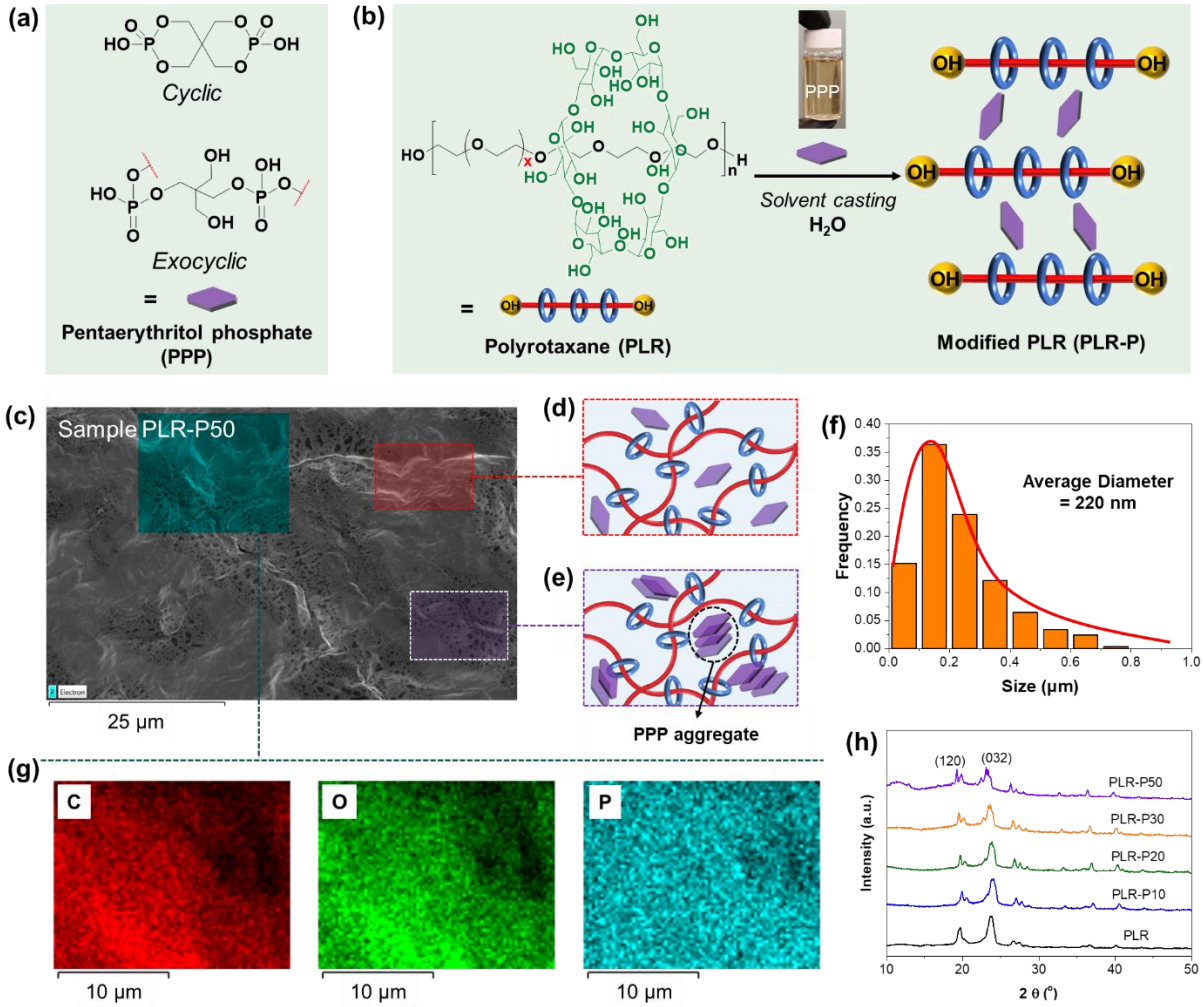


**Figure 1**. (a) Chemical structure of the PPP flame retardant, (b) PLR-Ps preparation route by solvent blending (PLRs and PPP were solvent casted in PTFE mold. The composition of the samples is listed in **Table S3**), (c) SEM image of sample PLR-P50, (d) dispersion illustration of P element without significant aggregation, (e) dispersion of P with significant aggregations, (f) particle size and distribution of PPP in PLR-P50, (g) EDS mapping of C, O and P, and (h) XRD curves of the PLR-Ps and PLR.

**Figure 1h** presents XRD patterns of the all PCMs. The two peaks at 2θ of about 19° and about 23° are respectively attributed to the (120) and (032) PEO crystals planes. The XRD results indicated that the introduce of PPP didn't make the PLR lose crystallinity, which ensures that the material can be used as a PCM for thermal storage. The crystallinity of the materials was calculated according to the DSC results and based on Equation (S1). The results were listed in **Table S3**. Typically, the crystallinity increased at first (sample PLR-P10) and then decreased gradually when the PPP contents was higher than 30 wt.%. The decreasing of crystallinity is because the impurities and plasticizing effects of PPP. The melting temperature ($T_m$), latent heat ($\Delta H_m$), solidification temperature ($T_s$), and crystallinity ($\varphi_c$) of the pure PLR and PLR-Ps were listed in **Table S3**. From the point of the crystallinity, the PPP acts as heterogeneous nucleating agent within an appropriate amount, which has a positive effect on the crystallization of PEO. Therefore, the crystallinity of sample PLR-P10 (58.17 %) is relative higher than that of PLR (57.39 %). When the PPP content continues to increase, the excess PPP acts as a plasticizer

and has a positive contribution to the elongation at break, but the modulus and tensile strength decrease significantly.

*2. Mechanical performance*

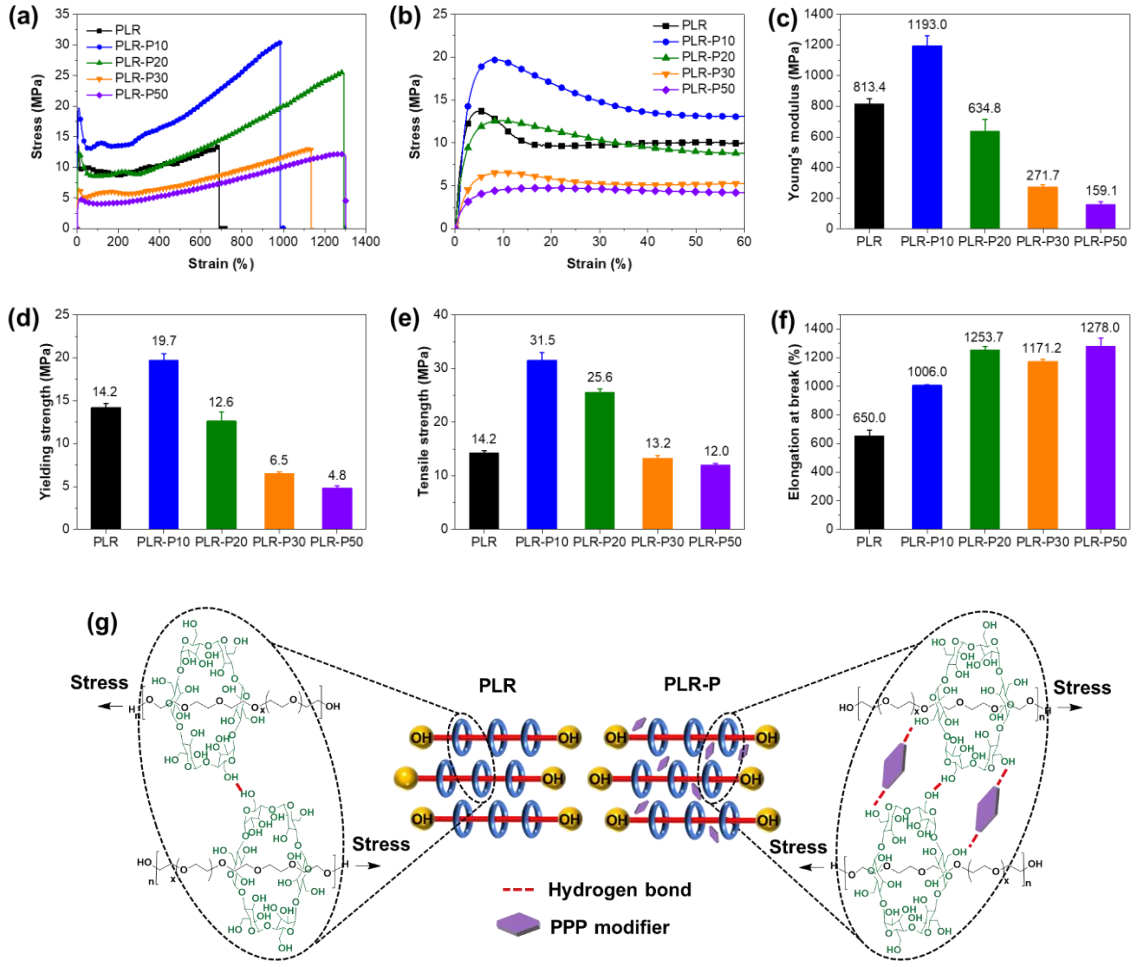


**Figure 2**. (a) Full range and (b) low strain region of stress-strain curves, (c) Young's moduli, (d) yielding strength, (e) tensile strength, (f) elongation of the PCM samples, and (g) the mechanical enhancement mechanism illustration.

**Figure 2a** presents stress–strain curves of the all PCMs. Detailed mechanical properties are listed in **Table S4**. The materials have obvious yielding phenomenon **(Figure 2b)** and significant strain hardening during the tensile process (Figure 2a). It is further found that with the PPP contents increase, the tensile strength, Young's modulus, and yielding strength of the material increased at first and then decreased gradually. All the Young's modulus, yielding strength and tensile strength follow the same trend (**Figure 2c-f**), among of which, PLR-P10 can reach the top value. Typically, Young's Modulus, tensile strength, elongation (%), and yielding strength are 1193.0 MPa, 31.5 MPa, 1006 %, and 19.7 MPa, respectively. For sample PLR-P10 and PLR-P20, the reason for the mechanical enhancement may be due to the well dispersion of PPP, the enhanced crystallinity (see the increase of crystallinity from DSC results), and the intramolecular hydrogen bond enhancement. Therefore, strengthening and toughening are realized simultaneously. With the further increase of PPP contents, the plasticization of the PPP fluid will be significantly reflected. Namely, the elongation increases, while Young's modulus

and tensile strength decrease significantly (Sample PLR-P30 and PLR-P50). As shown in **Figure 2g**, the interactions between α-CD and α-CD in PLR include (1) hydrogen bond between α-CD in both PLR and PLR-Ps (there are more hydrogen bonds in PLR-Ps due to the introduce of -OH rich PPP) and (2) steric hindrance between α-CD (as described in our previous work [10]). In addition, one of the significant advantages of liquid modifiers is the formability (shape change), which will dissipate some energy and make up for strain defects, so as to play an important role in maintaining the mechanical properties of materials during tension (as further illustrated in **Figure S7**).[23] Typically, the Micro-Nano PPP aggregates may act as an inter-pore bridge, resulting in a relative highly heterogeneous stress distribution, which ensures high mechanical performance under a high filling content (as high as 50 wt.%), which is the main reason why we prefer PPP, an oil like liquid, as a modifier rather than solid-state PPM.

*3. PCMs performance*

**Table 1**. Typical PCMs parameters

| Samples | Enthalpy efficiency (%) | Activation energy (ΔEa, kJ mol$^{-1}$) | Extent of Supercooling (ºC) | Heat lose (%) | Thermal conductivity (W·m$^{-1}$·K$^{-1}$) | Leakage |
|---|---|---|---|---|---|---|
| PLR | 99.9 | 571.1 | 11.4 | 2.1 | 0.28±0.01 | No |
| PLR-P10 | 99.1 | 352.3 | 11.1 | 0.4 | 0.36±0.03 | No |
| PLR-P20 | 102.9 | 257.5 | 11.8 | 0.6 | 0.37±0.02 | No |
| PLR-P30 | 94.2 | 445.0 | 13.9 | 1.1 | 0.41±0.05 | No |
| PLR-P50 | 74.8 | 300.6 | 14.6 | 2.6 | 0.47±0.06 | No |

The ΔEa can be calculated by Kissinger's Equation:[24]

$$\frac{d[ln(\varphi/T_P^2)]}{d(\frac{1}{T_P})} = -\frac{\Delta E_a(T)}{R} \quad (1)$$

where $\varphi$ is the heating rate, $T_P$ is the peak phase change temperature and R is the gas constant.

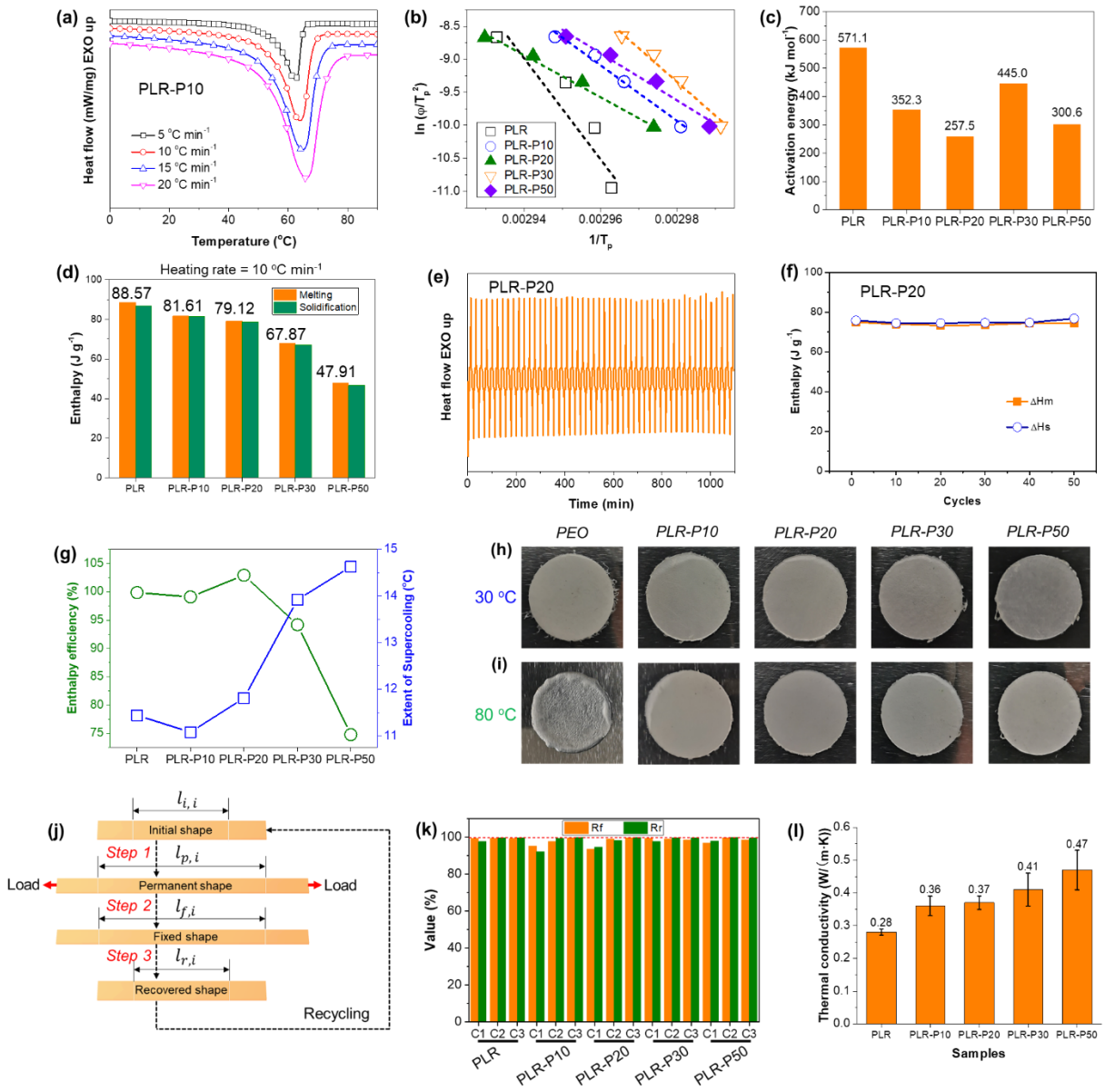


**Figure 3**. (a) DSC curves of sample PLR-P10 with different heating rates, (b) ln(Ø/Tp$^2$) versus 1/Tp plots; (c) $\Delta E_a$ of PLR and PLR-Ps; (d) melting and solidification enthalpies ($\Delta H_m$ values are shown in the Figure) of PCMs with different PPP contents; (e) DSC curves of composite PCMs after many times thermal cycling (PLR-P20 as a typical example); (f) the cycle stability (including melting and solidification enthalpies) of PLR-P20, (g) enthalpy efficiency and extent of supercooling trends with different PPP contents, and form stability of the samples: (h), 30 °C, and (i) 80 °C for 2 h, (j) Qualitative characterization illustration of the shape memory properties, (k) Shape fix ratio ($R_f$) and shape recovery ratio ($R_r$) values, and (l) thermal conductivity results of the PCMs.

**Figure 3a** shows the melting curves of sample PLR-P10 determined at different heating rates. The related curves of other PCMs are shown in **Figure S10-12**. **Figure 3b** presents the Kissinger plots based on the data corresponding to **Figure 3a** and Figure S10-12. The Tp of all the samples under different heating and cooling rate were all summarized in **Table S6**. From the slope in the plots of $ln\left(\frac{\varphi}{T_P^2}\right)$ against $\frac{1}{T_P}$, the following Ea values were calculated: $E_{a,PLR}$=571.1 kJ mol$^{-1}$ for pure PLR, $E_{a,\ PLR\text{-}}$

$_{P10}$=352.3 kJ mol$^{-1}$, $E_{a,\ PLR\text{-}P20}$=257.5 kJ mol$^{-1}$, $E_{a,\ PLR\text{-}P30}$=445.0 kJ mol$^{-1}$ and $E_{a,\ PLR\text{-}P50}$=300.6 kJ mol$^{-1}$ for PLR-P10, PLR-P20, PLR-P30 and PLR-P50, respectively (**Table 1)**. It is found that all the $\Delta E_a$ of the PLRs are much lower than that of pure PLR, which maybe because the PPP will promote the mobility process (especially the beginning) of PEO chain in the PCMs.

The extent of supercooling (ΔT, $^{o}$C) can be evaluated by the following equation:

$$\Delta T = T_{m,onset} - T_{s,onset} \quad (2)$$

where $T_{m,onset}$ and $T_{s,onset}$ are onset melting temperature and onset solidifying temperature, respectively. Based on equation (2), the ΔT of the PCMs is calculated and listed in **Table 1**. The extent of supercooling increased with the increase of PPP contents, which indicated that the high contents of PPP can hinder the nucleation process of PEO molecular chain to a certain extent.

Furthermore, the Enthalpy efficiency of PCMs can be determined by equation 3, [8] [29]

$$Enthalpy\ efficiency\ \% = \frac{\Delta H_m}{\omega \Delta H_{PCM}} \times 100\ \% \quad (3)$$

where, $\Delta H_m$ was the Enthalpy of the PCMs. $\Delta H_{PCM}$ represents the Enthalpy of pure PLR, and $\omega$ (%) represents the weight percentage of PLR in the PCMs. The percentage of heat lose ($\eta$, %) was calculated by equation 4:

$$\eta = \frac{\Delta H_m - \Delta H_s}{\Delta H_m} \times 100\ \% \quad (4)$$

where, $\Delta H_m$ and $\Delta H_s$ were the latent heat and solidification enthalpy of the PCMs, respectively.

Both the Enthalpy efficiency % results and the η for all the PCM samples are calculated and listed in **Table 1**. The $\eta$ for all the PCMs were quite low (<2.59%), indicating PPP will not significantly induce the heat loss of PEO in PCMs. **Table S3** summarized the thermal properties of PLR and PLR-Ps, such as the $\Delta H_m$, $T_{m,onset}$, $\Delta H_s$, and $T_S$. The PCMs exhibited a phase change enthalpy of 47.91~81.86 J g$^{-1}$, which is shown in Figure 3d and listed in Table S3, and high enthalpy efficiency (~100 % for PLR-P10 and PLR-P20). The PCMs had high cycle performance because the main parameters for PCM (such as $\Delta H_m$ and $\Delta H_s$) remained virtually unchanged (**Figure 3e, f,** and **Table 1**). The PLR films are therefore regarded as high-performance shape-stable PCMs. However, as shown in **Figure 3g**, because the crystallinity of PLR decreased a lot with high filling content of PPP, the enthalpy efficiency also decreased significantly (especially for sample PLR-P50). As described above, the PPP may hinder the nucleation process of PEO, giving rise to the gradually increased extent of supercooling.

The photos of PLR and PLR-Ps using hot stage treatment at different temperature are shown in **Figure 3h**, **Figure 3i** and **Figure S9**. PEO gradually began to melt when the temperature reached the $T_m$, but the PLR based PCMs showed no significant changes in appearance and no leakage was detected for all the PLR-PCMs. These results indicate that the PLRs has good shape stability.

The PCMs perform outstanding shape memory properties. The examination of heat-induced SMPs using the procedure described in the supporting information and shown in **Figure 3j**. **Figure 3k** and **Table S7** showed the values for shape fixity ($R_f$) and shape recovery ($R_r$) within 3 cycles (C1, C2 and C3) for all the PCMs. As it can be seen, the $R_f$ is with ~98 %, and the $R_r$ is with ~99 %. Moreover, as shown in **Figure 3l**, the thermal conductivity from 0.28 W m$^{-1}$ K$^{-1}$ for PLR to 0.47 W m$^{-1}$ K$^{-1}$ for PLR-P50. The significantly improved thermal conductivity will be conducive to the thermal transfer and heat-harvesting rate of the PCM, and improve the performances in electrical devices thermal regulation accordingly.

*4. Fire-safety and application example*

PPP possess excellent fire-resistant property owing to their intrinsic nonflammability. Hence, PPP can be used to protect flammable objects. The combustion process of sample PLR-P10, PLR-P20 and PLR-P30 were similar to that of PLR-P50, and provided in Supporting Information (**Figure S8**). All the samples finished the burning process in ten seconds. In a control group, sample PLR produced significant molten drop (at 6s, **Figure 4a**). All the modified samples can generate a stable char residual (**Figure 4b**) and no dripping. This can effectively guarantee to slow down the spread of fire in the practical process, and enhance the fire safety to a certain extent accordingly.

Subsequently, TGA were carried out to determine the thermal stability of the PCMs and further confirm the enhanced char-forming ability. The corresponding results are presented in **Figure 4c** and listed in **Table S5**. All the PCMs mainly underwent a two-step degradation process. The weight loss near 100 $^{o}$C is mainly due to absorbed water (Region A in Figure 4c). It is clearly seen that all the PLR-Ps begin to decompose after 170 $^{o}$C. Even if the PCM-Ps decomposed in advance in comparison with PLR, the decomposition temperature also can ensure the thermal stability of the material in the service temperature range, so as to meet the general requirements of PCM. By comparing the decomposition curves of pure PPP, we know that the weight loss in the first stage (170 ~ 220 $^{o}$C) and the final weight loss after 500 $^{o}$C are all due to the PPP decomposition. As it is reported, the decomposition starts earlier, following a different pathway with more incomplete decomposition and a higher char residue. [30] This was similar to the ordinary phosphorous containing modifiers, which could reduce the degradation temperature of the PCMs and changed the decomposition history. [31, 32] After modification, char of the material increases significantly (from 1.1% of PLR to 22.9 % of PLR-P50), which is consistent with the results of combustion test (Figure 4a-4b).

Limiting Oxygen Index (LOI) and UL-94 vertical burning tests were recorded to study the fire safety of the PCMs. The results are shown in **Figure 4d-f** and **Table 2**. After the addition of 50 wt.% PPP, the LOI values increased significantly from 20.8% to 33.0% and the PCM reached a V-0 rating in the UL-94 test. In addition, a cone calorimeter was implemented to further evaluate the fire behaviors of the PCMs in real combustion situations. Figure 4d–e presented the heat release rate (HRR) and total heat release (THR) curves of the PCM composites. The peak of HRR (pHRR) and THR values of the PLR-P50 were only 310 kW/m$^{-2}$ and 40.1 MJ/m$^{-2}$, with a remarkable decrease of 52.42% and 39.11%, respectively, compared to those of pure PLR. The char morphology of the PCMs after CONE test are shown in **Figure S13**, which is consistent with the char residue that obtained from TGA tests. Furthermore, we listed some parameters of reported PCMs, as shown in **Table S8**. As it can be seen, at present, the reports of systematic research on the flame retardant performance of PCM are relatively limited, so the progress of this work is reflected in the comprehensive report of a new fire safety PCM. The PCMs were fabricated by using only water as the solvent. We believe that it is green and environment friendly process.

**Table 2.** The typical parameters of TGA, Cone Calorimeter testing, UL-94 and LOI

| Samples | [a]Char residue (%) | pHRR (kW m$^{-2}$) | THR (MJ m$^{-2}$) | LOI (%) | UL-94 | Dripping |
|---|---|---|---|---|---|---|
| PLR | 1.1 | 652 | 65.9 | 20.8 | No rating | Yes |
| PLR-P10 | 3.9 | 369 | 54.5 | 26.2 | No rating | No |
| PLR-P30 | 13.6 | 343 | 48.7 | 29.6 | No rating | No |
| PLR-P50 | 22.9 | 310 | 40.1 | 33.0 | V0 | No |

[a] The values are obtained from TGA results.

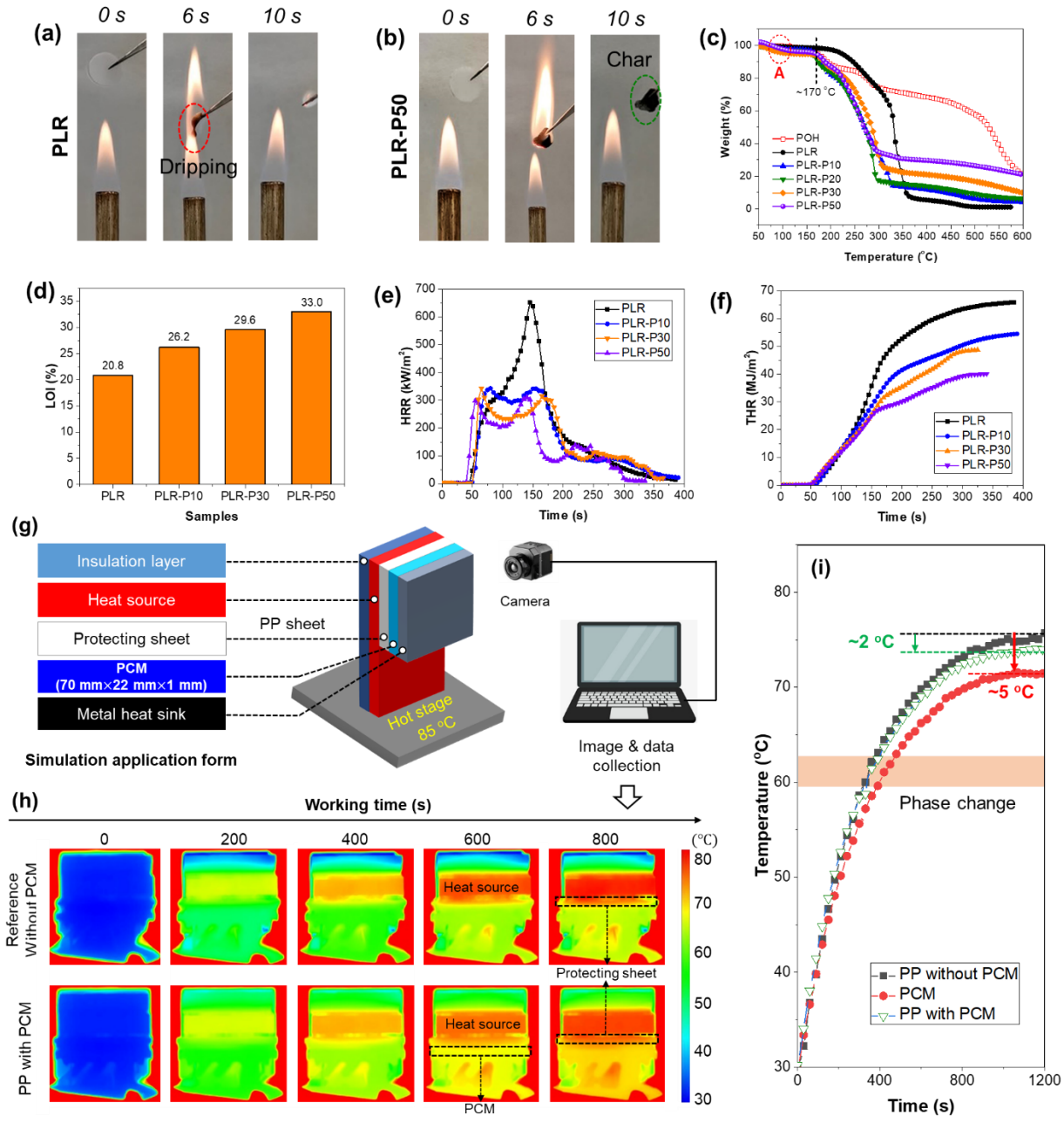


**Figure 4**. (a) Combustion process of sample PLR, (b) combustion process of sample PLR-P50, (c) TGA curves of PPP, PLR, and modified PLRs, (d) HRR curves of PLR, and modified PLRs, (e) THR curves of PLR, and modified PLRs, (f) LOI values of PLR, and modified PLRs. (g) illustration of the experimental stack structure of the device, test process and sample test diagram: including sample heating, signal acquisition and data storage, (h) IR images of the devices during heating at 85 °C, (i) the heating curves of the devices that without PCM and with PLR-P50.

A typical application of PCM is the heat management of electronic devices. In order to meet the needs of convenient laboratory testing, we designed a schematic structure (semi-SSD based device,

**Figure 4g**). As shown in Figure 4g, the insulation layer (wood sheet, 5 mm in thickness), heating source (a metal sheet with 5 mm in thickness), protecting sheet (Polypropylene (PP) with 2 mm in thickness), PCM (70 mm×22 mm×1 mm in thickness, which is the same as the size of commercial product) and the metal heatsink stacked together to prepare the testing device. **Figure 4h** shows the IR images of different samples at different heating time. We can further obtain the measured temperature change heating curves, as shown in **Figure 4i**. As shown in **Figure 4i**, the endothermic and exothermic state of the analog device can form a relatively stable equilibrium state at last. During the whole heating cycle, sample PLR-P50 in this study showed significantly better temperature control state than both the blank samples and commodities. Specifically, the temperature of the protecting part with PCM was significantly lower than that of blank sample and commercial PCM. Furthermore, there was no significant difference in the initial stage (linear sensitive heating stage, Figure 4i). After entering the phase change region, the temperature difference gradually appears and maintain about 2 $^{o}$C. The difference is due to the enthalpy effect of PLR-P50 phase transition, which plays a role in temperature regulation for a long time.

## Conclusions

PLR with different PPP contents (10 wt.%~50 wt.%) were successfully prepared via facile blending method. All the Young's modulus, tensile strength and yielding strength of the modified PCMs increased at first and then decreased. Typically, the Young's modulus, yielding strength and tensile strength of the PLR were 826.7 MPa, 14.2 MPa and 14.2 MPa, respectively, and remarkably increased to 1193.0 MPa, 19.7 MPa, and 31.5 MPa respectively, with the addition of 10 wt.% of PPP. Elongation for all modified PCMs was higher than 1000 %. The char-forming ability of PLR is significantly improved. Specifically, the char residual increased from 1.1 % to 22.9 % according to TGA. Thermal analysis shows that the fire safety of PLR is significantly improved. Specifically, the pHRR could decrease by 52.42 %, THR decreased by 39.11 %; the LOI increased from 20.8 % to 33.0 %. Moreover, the stable char residual will be formed during combustion process. The PCMs possess high shape-fixing ($R_f$~98 %) and recovery properties ($R_r$~99 %). Further with the excellent form-stability, good cycle characteristics and sustainable nature of PLR matrix, the modified PLR films are therefore promising sustainable, ultra-flexible, form-stable and fire safe PCMs for thermal energy storage. Notably, the PPP modified PCM can realize UL-94 V0 rating, excellent leakage-proof and form-stability, significantly improved thermal conductivity, it therefore performed obvious temperature regulation function in a simulated solid-state disk temperature reduction.

## Declaration of Competing Interest

The authors declare that they have no known competing financial interests or personal relationships that could have appeared to influence the work reported in this paper.

## CRediT authorship contribution statement

**Guang-Zhong Yin**: Conceptualization, Methodology, Validation, Data curation, Writing-original draft, Writing-review & editing, Project administration. **Alba Marta López**: Data curation, Investigation, Writing-review & editing. **Xiao-Mei Yang**: Data curation, Writing-review & editing. **Wen Ye**: Formal analysis, Writing-review & editing. **Baoyun Xu**: Formal analysis, Writing-review & editing. **Jose Hobson**: Data curation, Writing-review & editing. **De-Yi Wang**: Project administration, Methodology, Writing-review & editing, Supervision, Funding acquisition.

**Acknowledgment**

The authors acknowledge the financial support provided by BIOFIRESAFE Project funded by Ministerio De Ciencia E Innovación (MINECO), Spain with Project number: PID2020-117274RB-I00BIOFIRESAFE.

**References**

[1] K. Iqbal, A. Khan, D. Sun, M. Ashraf, A. Rehman, F. Safdar, A. Basit, H.S. Maqsood, Phase change materials, their synthesis and application in textiles—a review, The Journal of The Textile Institute 110(4) (2019) 625-638.

[2] T.R. Whiffen, S.B. Riffat, A review of PCM technology for thermal energy storage in the built environment: Part I, International Journal of Low-Carbon Technologies 8(3) (2012) 147-158.

[3] J. Li, Z. Cheng, M. Zhu, A. Thomas, Y. Liao, Facile Synthesis of Nitrogen-Rich Porous Organic Polymers for Latent Heat Energy Storage, ACS Applied Energy Materials 1(11) (2018) 6535-6540.

[4] B. Wang, G. Li, L. Xu, J. Liao, X. Zhang, Nanoporous Boron Nitride Aerogel Film and Its Smart Composite with Phase Change Materials, ACS Nano 14(12) (2020) 16590-16599.

[5] C. Yan, N. Meng, W. Lyu, Y. Li, L. Wang, Y. Liao, Hierarchical porous hollow carbon spheres derived from spirofluorene- and aniline-linked conjugated microporous polymer for phase change energy storage, Carbon 176 (2021) 178-187.

[6] Z. Cai, J. Liu, Y. Zhou, L. Dai, H. Wang, C. Liao, X. Zou, Y. Chen, Y. Xu, Flexible phase change materials with enhanced tensile strength, thermal conductivity and photo-thermal performance, Solar Energy Materials and Solar Cells 219 (2021) 110728.

[7] Q. Huang, X. Li, G. Zhang, J. Deng, C. Wang, Thermal management of Lithium-ion battery pack through the application of flexible form-stable composite phase change materials, Applied Thermal Engineering 183 (2021) 116151.

[8] P. Cheng, H. Gao, X. Chen, Y. Chen, M. Han, L. Xing, P. Liu, G. Wang, Flexible monolithic phase change material based on carbon nanotubes/chitosan/poly(vinyl alcohol), Chemical Engineering Journal 397 (2020) 125330.

[9] Y. Kou, K. Sun, J. Luo, F. Zhou, H. Huang, Z.-S. Wu, Q. Shi, An intrinsically flexible phase change film for wearable thermal managements, Energy Storage Materials 34 (2021) 508-514.

[10] G.-Z. Yin, J. Hobson, Y. Duan, D.-Y. Wang, Polyrotaxane: New generation of sustainable, ultra-flexible, form-stable and smart phase change materials, Energy Storage Materials 40 (2021) 347-357.

[11] L. Li, G. Wang, C. Guo, Influence of intumescent flame retardant on thermal and flame retardancy of eutectic mixed paraffin/polypropylene form-stable phase change materials, Applied Energy 162 (2016) 428-434.

[12] G. Song, S. Ma, G. Tang, Z. Yin, X. Wang, Preparation and characterization of flame retardant form-stable phase change materials composed by EPDM, paraffin and nano magnesium hydroxide, Energy 35(5) (2010) 2179-2183.

[13] P. Zhang, Y. Hu, L. Song, J. Ni, W. Xing, J. Wang, Effect of expanded graphite on properties of high-density polyethylene/paraffin composite with intumescent flame retardant as a shape-stabilized phase change material, Solar Energy Materials and Solar Cells 94(2) (2010) 360-365.

[14] M.J. Mochane, A.S. Luyt, Synergistic effect of expanded graphite, diammonium phosphate and Cloisite 15A on flame retardant properties of EVA and EVA/wax phase-change blends, Journal of Materials Science 50(9) (2015) 3485-3494.

[15] M.J. Mochane, A.S. Luyt, The effect of expanded graphite on the thermal stability, latent heat, and flammability properties of EVA/wax phase change blends, Polymer Engineering & Science 55(6) (2015) 1255-

1262.
[16] J. Wang, Y. Wang, R. Yang, Flame retardance property of shape-stabilized phase change materials, Solar Energy Materials and Solar Cells 140 (2015) 439-445.
[17] E.N. Kalali, X. Wang, D.-Y. Wang, Functionalized layered double hydroxide-based epoxy nanocomposites with improved flame retardancy and mechanical properties, Journal of Materials Chemistry A 3(13) (2015) 6819-6826.
[18] E.N. Kalali, X. Wang, D.-Y. Wang, Multifunctional intercalation in layered double hydroxide: toward multifunctional nanohybrids for epoxy resin, Journal of Materials Chemistry A 4(6) (2016) 2147-2157.
[19] G. Makhlouf, A. Abdelkhalik, M.A. Hassan, Combustion toxicity of polypropylene containing melamine salt of pentaerythritol phosphate with high efficiency and stable flame retardancy performance, Process Safety and Environmental Protection 138 (2020) 300-311.
[20] X. Chen, C. Ma, C. Jiao, Synergistic effects between iron–graphene and melamine salt of pentaerythritol phosphate on flame retardant thermoplastic polyurethane, Polymers for Advanced Technologies 27(11) (2016) 1508-1516.
[21] T. Zhou, H. Xu, L. Cai, J. Wang, Construction of anti-flame network structures in cotton fabrics with pentaerythritol phosphate urea salt and nano SiO2, Applied Surface Science 507 (2020) 145175.
[22] S. Wang, L. Qian, F. Xin, The synergistic flame-retardant behaviors of pentaerythritol phosphate and expandable graphite in rigid polyurethane foams, Polymer Composites 39(2) (2018) 329-336.
[23] G.-Z. Yin, X. Yang, Z. Zhou, Q. Li, A Green Pathway to Adjust the Mechanical Properties and Degradation Rate of PCL by Blending Bio-sourced Poly (Glycerol-Succinate) Oligoesters, Materials Chemistry Frontiers (2017).
[24] X. Chen, H. Gao, G. Hai, D. Jia, L. Xing, S. Chen, P. Cheng, M. Han, W. Dong, G. Wang, Carbon nanotube bundles assembled flexible hierarchical framework based phase change material composites for thermal energy harvesting and thermotherapy, Energy Storage Materials 26 (2020) 129-137.
[25] Y.-N. Chen, C. Jiao, Y. Zhao, J. Zhang, H. Wang, Self-Assembled Polyvinyl Alcohol–Tannic Acid Hydrogels with Diverse Microstructures and Good Mechanical Properties, ACS Omega 3(9) (2018) 11788-11795.
[26] Y. Yang, X. Zhao, J. Yu, X. Chen, X. Chen, C. Cui, J. Zhang, Q. Zhang, Y. Zhang, S. Wang, Y. Cheng, H-Bonding Supramolecular Hydrogels with Promising Mechanical Strength and Shape Memory Properties for Postoperative Antiadhesion Application, ACS Applied Materials & Interfaces 12(30) (2020) 34161-34169.
[27] Y.-N. Chen, L. Peng, T. Liu, Y. Wang, S. Shi, H. Wang, Poly(vinyl alcohol)–Tannic Acid Hydrogels with Excellent Mechanical Properties and Shape Memory Behaviors, ACS Applied Materials & Interfaces 8(40) (2016) 27199-27206.
[28] S. Yang, Y. Zhang, T. Wang, W. Sun, Z. Tong, Ultrafast and Programmable Shape Memory Hydrogel of Gelatin Soaked in Tannic Acid Solution, ACS Applied Materials & Interfaces 12(41) (2020) 46701-46709.
[29] X. Zhang, H. Liu, Z. Huang, Z. Yin, R. Wen, X. Min, Y. Huang, Y. Liu, M. Fang, X. Wu, Preparation and characterization of the properties of polyethylene glycol @ $Si_3N_4$ nanowires as phase-change materials, Chemical Engineering Journal 301 (2016) 229-237.
[30] R.S. Kappes, T. Urbainczyk, U. Artz, T. Textor, J.S. Gutmann, Flame retardants based on amino silanes and phenylphosphonic acid, Polymer Degradation and Stability 129 (2016) 168-179.
[31] S. Hao, W. Zhu, H. Huang, M. Yang, J. Zhang, A Phosphorous-Aluminium-Nitride Synergistic Flame Retardant to Enhance Durability and Flame Retardancy of Cotton, ChemistrySelect 4(47) (2019) 13952-13958.
[32] P. Zhu, S. Sui, B. Wang, K. Sun, G. Sun, A study of pyrolysis and pyrolysis products of flame-retardant cotton fabrics by DSC, TGA, and PY–GC–MS, Journal of Analytical and Applied Pyrolysis 71(2) (2004) 645-655.